Eur. Phys. J. A **24**, 389–394 (2005)
DOI 10.1140/epja/i2004-10148-y

THE EUROPEAN PHYSICAL JOURNAL A

Momentum-dependent mean field in π_0 production in Nb + Nb collisions

G. Russo[1], A. Insolia[1,a], U. Lombardo[1], and N.G. Sandulescu[2]

[1] Department of Physics and Astronomy, University of Catania and INFN, Via S. Sofia 64, I-95123 Catania, Italy
[2] Institute of Atomic Physics, Bucharest Magurele, POB MG 6, Romania

Received: 26 June 2004 / Revised version: 18 February 2005 /
Published online: 2 June 2005 –
Communicated by A. Molinari

Abstract. The Boltzmann-Nordheim-Vlasov (BNV) equation has been solved by using a microscopic momentum-dependent (MD) nuclear mean field. This potential has been calculated in the framework of the self-consistent Brueckner theory up to the second order in the G-matrix. Comparison with the so-called soft and stiff Equation of State (EOS) is presented, using the Skyrme force. Calculations have been performed for the ^{93}Nb + ^{93}Nb reaction at $E_{\rm lab} = 100, 250, 400$ A MeV. Our results show that the sub-threshold π_0 production cross-section is very sensitive to the momentum-dependent mean field, resulting, at the lowest energy, in a total cross-section a factor of 7 larger than that obtained with a local potential. The effect decreases as the bombarding energy increases.

PACS. 21.60.Jz Hartree-Fock and random-phase approximations – 25.70.-z Low and intermediate energy heavy-ion reactions

1 Introduction

The question whether the equation of state (EoS) of nuclear matter is stiff or soft is still largely controversial. No clear answer has been given so far either in Heavy-Ion Collisions (HIC) and in astrophysics. The idea that the sideward flows observed in HIC at intermediate energy could be a signature of a high incompressibility of nuclear matter has received a strong support by a lot of dynamical simulations using phenomenological mean fields such as the stiff Skyrme force. But it has been very soon recognized that similar predictions can be obtained also by using a soft EoS whose mean field is momentum dependent (MD) [1,2]. The momentum dependence reflects the non-local nature of the optical potential in elastic nucleon scattering and results in a nuclear mean field which becomes less and less attractive as far as its momentum increases and repulsive at k larger than 3–4 fm^{-1}.

The mean fields used in dynamical simulations of HIC, as well as their MD extensions, do not rely on a microscopic basis. This drawback becomes more serious as far as one wants to introduce in the equations an in-medium cross-section consistent with the used mean field.

The potential we used in our calculations has been derived from the Brueckner-Bethe-Goldstone (BBG) approach, with the Paris potential as input for the realistic interaction [3]. To the Brueckner-Hartree-Fock (BHF) term, describing the polarization potential, we added the second-order contribution in the G-matrix. This correction includes the two-particle–two-hole excitations probing the ground-state correlations in nuclear matter.

In this paper we will study π_0 production in ^{93}Nb + ^{93}Nb collisions at three bombarding energies, $E_{\rm lab} = 100, 250, 400$ A MeV, exploiting the whole range of impact parameters.

The mean field will be discussed in the next section while applications and conclusions are reported in the last two sections.

2 Momentum-dependent mean field from the Brueckner theory

In this section we describe the formalism of the Brueckner-Bethe-Goldstone (BBG) theory [4,5]. The starting point of the BBG theory is the Brueckner reaction matrix G, which satisfies the Bethe-Goldstone equation,

$$G(\rho,\beta;\omega) = v_{NN} + v_{NN} \times \sum_{k_1 k_2} \frac{|k_1 k_2\rangle Q(k_1,k_2)\langle k_1 k_2|}{\omega - \epsilon(k_1) - \epsilon(k_2) + i\eta} G(\rho,\beta;\omega)\ , \qquad (1)$$

where v_{NN} is the two-body nuclear interaction and ω the starting energy. Here $k \equiv (\vec{k},\sigma,\tau)$ denotes s.p. momentum, z-components of spin and isospin, respectively. ρ is

[a] e-mail: Antonio.Insolia@ct.infn.it

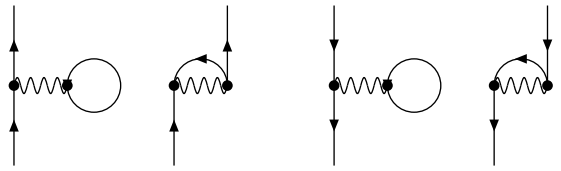

Fig. 1. First-order particle and hole potentials with their exchange terms. Wiggles are G-matrix elements.

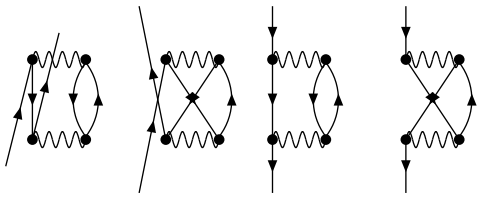

Fig. 2. Second-order particle and hole potentials with their exchange terms. Wiggles are G-matrix elements.

the total density of the system and $\beta = \frac{N-Z}{A}$ is the isospin asymmetry parameter. The G-matrix can be considered as an in-medium effective interaction between two nucleons. The surrounding nucleons renormalize the bare NN interaction via the Pauli blocking and the nuclear mean field. The Pauli operator, defined as

$$Q(k_1, k_2) = [1 - n(k_1)][1 - n(k_2)] \ , \tag{2}$$

prevents two nucleons in intermediate states from scattering into states inside their respective Fermi seas. By $n(k)$ we denote the Fermi distribution function, which at zero temperature is given by the step function $\theta(k - k_{\rm F}^{\tau})$ (uncorrelated ground state), being $k_{\rm F}^{\tau}$ the Fermi momentum of the nucleon with isospin τ. The single-particle (s.p.) energy

$$\epsilon(k) = \frac{\hbar^2 k^2}{2m} + U(k) \ , \tag{3}$$

appearing in the energy denominator of eq. (1), involves the *auxiliary* potential $U(k)$, which controls the convergence rate of the hole-line expansion. Within the BHF approximation the auxiliary potential is defined as

$$U(k) = \sum_{k'} n(k') {\rm Re} \langle kk'|G(\epsilon(k) + \epsilon(k'))|kk'\rangle_A \ . \tag{4}$$

Here we adopt the continuous choice [6], which extends the definition of $U(k)$ to *any* k. This choice for the auxiliary s.p. potential makes the convergence of the hole-line expansion much faster than other choices [7].

The self-energy $M(k, \omega) = V(k, \omega) + iW(k, \omega)$, whose real part can be identified as the potential energy felt by a nucleon, can be expanded in a perturbation series according to the number of hole lines [8,9] and various terms of this expansion can be represented by means of Goldstone diagrams shown in figs. 1 and 2.

The quasi-particle energy $E(k)$ is the solution of the energy-momentum relation

$$E(k) = \frac{\hbar^2 k^2}{2m} + V(k, E(k)) \ . \tag{5}$$

To the lowest order in the hole-line expansion the self-energy is given by (diagrams in fig. 1)

$$M_1(k, \omega) = \sum_{k'} n(k') \langle kk'|G(\omega + \epsilon(k'))|kk'\rangle_A . \tag{6}$$

In the previous expression as in what follows the explicit summation over the isospin index on the right-hand side will be understood and thus omitted. For more details we refer to [9]. In this approximation the quasi-particle energy E_1 coincides with the BHF s.p. energy given by eqs. (3) and (4), *i.e.*, $E_1 = \epsilon(k)$.

The next contribution to the perturbative expansion of the self-energy is given by the so-called *rearrangement* term $M_2(k, \omega)$ [6]. The associated Goldstone diagrams are represented by the diagrams of fig. 2. M_2 is a second-order diagram in the G-matrix and accounts for particle-hole excitations in nuclear matter. Its expression reads

$$M_2(k, \omega) = \frac{1}{2} \sum_{k'} (1 - n(k')) \times \sum_{k_1 k_2} n(k_1) n(k_2) \frac{|\langle kk'|G(\epsilon(k_1) + \epsilon(k_2))|k_1 k_2\rangle_A|^2}{\omega + \epsilon(k') - \epsilon(k_1) - \epsilon(k_2) - i\eta} , \tag{7}$$

where $\epsilon(k)$ is the s.p. spectrum in BHF approximation given by eqs. (3) and (4). In this approximation for the self-energy the quasi-particle energy (5) is given by the approximate relation

$$E_2(k) = E_1(k) + Z_2(k) V_2(k) = \frac{\hbar^2 k^2}{2m} + V_1(k) + Z_2(k) V_2(k) \ , \tag{8}$$

where

$$Z_2(k) = \left\{ 1 - \frac{\partial}{\partial \omega} \Big[V_1(k, \omega) + V_2(k, \omega) \Big] \right\}^{-1}_{\omega = E_1(k)} \tag{9}$$

is an approximation of the *quasi-particle strength* for asymmetric nuclear matter

$$Z(k) = \left\{ 1 - \frac{\partial}{\partial \omega} \Big[V(k, \omega) \Big] \right\}^{-1}_{\omega = E(k)} . \tag{10}$$

In the preceding equations V_1 and V_2 are the on-shell values of M_1 and M_2, respectively, and represent the mean field employed in our dynamical simulations. They have been calculated in the framework of the Brueckner theory.

The neutron (proton) s.p. potentials (V and W are the real and imaginary part, respectively) are plotted *vs.* momentum in figs. 3 and 4 in asymmetric nuclear matter at

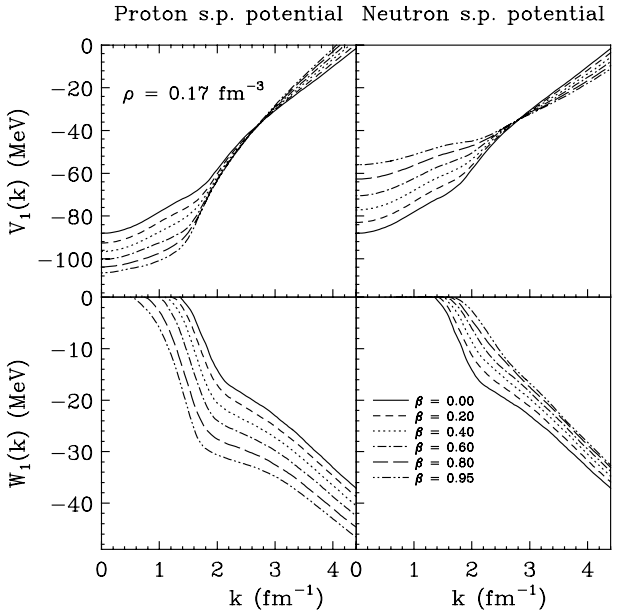

Fig. 3. Real part (upper panels) and imaginary part (lower panels) of the first-order single-particle potentials M_1 for proton (left panel) and neutron (right panel) for different asymmetry parameters at density $\rho = 0.17\,\mathrm{fm}^{-3}$.

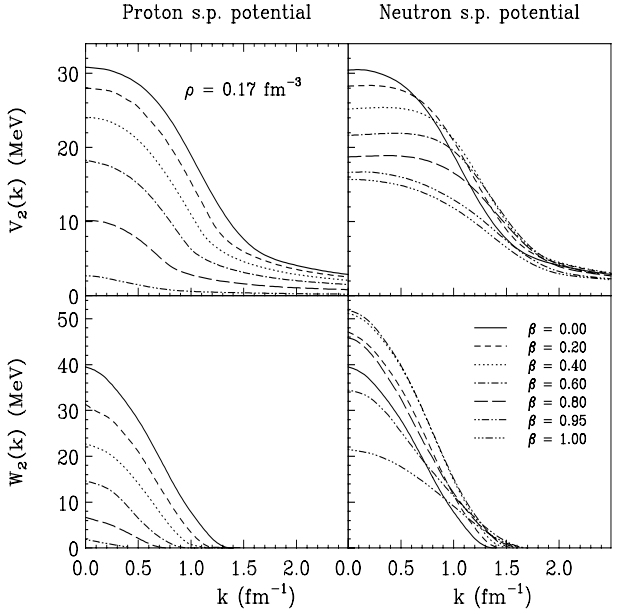

Fig. 4. Real part (upper panels) and imaginary part (lower panels) of the second-order single-particle potentials M_2 for proton (left panel) and neutron (right panel) for different asymmetry parameters at density $\rho = 0.17\,\mathrm{fm}^{-3}$.

the saturation density for the first-order and second-order expansions, respectively, for a few values of the asymmetry parameter β [9]. The realistic interaction adopted in the calculations is the $AV14$ [10]. The combination of the two terms produces a MD mean field which exhibits a flat behavior for k up to k_F. This means that, for low-momentum events, the momentum dependence is of no influence, whereas it results in a strong extra-repulsion in the momentum range above the Fermi energy.

Within the present BBG approach, higher-order corrections were recently calculated [9] as well as applications in transverse-flow calculations [11]. The inclusion of the third-order contributions in the G-matrix expansion do not produce major modifications in the microscopic mean field [12].

Those higher-order corrections were not included in the mean field used in the present paper and we refer to the figs. 1a, b of ref. [11] for additional details of the density and momentum dependence of the potential. It is worthwhile to stress that the MD potential obtained from our BBG approach is parameter free. In the momentum range up to k_F, the potential does not appreciably vary. This momentum range is of great relevance to the EoS, because all physical quantities are contributed only from inside the Fermi sphere, at least at zero temperature.

The differences in the momentum dependence are quite evident, not only in the absolute value, but also in the slope. The momentum profile of the BBG potential is flat in the region of low and high momenta, giving there a vanishing momentum gradient in the BNV equation. The main effects have to be expected in the intermediate region, where the slope is the steepest.

3 Kinetic calculations

A semiclassical dynamical approach based on the BNV equation has been widely used to study the heavy-ion collisions at intermediate energy. In this framework, the nuclear many-body system is described by means of a time evolution equation for the one-body phase-space distribution function $f(\vec{r},\vec{p},t)$ in a dynamics ruled by the competition of mean field and two-body collisions effects, namely

$$\frac{\partial f}{\partial t} + \{f,h\} = I_\mathrm{coll}(f)\,, \tag{11}$$

where $\{f,h\}$ represent the Poisson brackets, h is the self-consistent single-particle Hamiltonian including the one-body momentum-dependent mean-field potential derived in sect. 2 and defined as

$$h(\vec{r},\vec{p},t) = \frac{p^2}{2m} + V(\vec{r},\vec{p},t), \tag{12}$$

where

$$V(\vec{r},\vec{p},t)$$

is either the soft (hard) local Skyrme potential or the first- and second-order single-particle potential ($M_1 + M_2$) defined in the previous section. Finally, I_coll is the collision integral assumed of Uehling-Uhlembeck type.

In the next section a very brief account on the pion production calculation will be given. Here we will discus the BNV equation solution method. The study of heavy-ion collisions by means of eq. (11) is essentially a numerical task which is generally solved using the pseudo-particles method [13], in which the one-body phase-space distribution function is represented by a collection of N test

particles, whose coordinates and momenta are evolved individually with a time step Δt. In the actual numerical simulations, the BNV equation is separated into a classical Hamilton's equation of motion for the propagation of the pseudo-particles, which are governed on the one hand, by an appropriate mean field and, on the other hand, by the stochastic two-body collisions caused by the residual nucleon-nucleon (NN) interaction.

Therefore, there are two essential ingredients: the mean-field potential and the in-medium NN scattering cross-section. In our calculation soft and hard local Skyrme potential (soft and hard cases correspond to compressibility $K = 200$ MeV or $K = 380$ MeV, respectively) and the microscopic momentum-dependent mean field are used for a comparison.

The test particles are described in terms of Gaussian functions, both in coordinate and momentum space with a fixed widths σ_r and σ_p [14]. The ground state is prepared by a Monte Carlo sampling the phase space with a variational self-consistent procedure to reproduce the nuclear binding energy. The collision integral is treated stochastically allowing the test particles to undergo collisions with a probability proportional to the Pauli-blocking–corrected nucleon-nucleon cross-section. The collisional criterion for the test particles is that based on the local-mean-path concept [8,9].

The two parameters entering the computer simulation of the collision integral are the number N of test particles per nucleon and the integration time step. Typically $N \geq 50$ Gaussian packets are needed to smoothly represent an observable such as the position or momentum distribution, while for steps $\Delta t \leq 1.0$ fm/c, the results do not depend very much on the time step of the simulation.

In our calculations, numerical convergence was assured with $N = 100$ and $\Delta t = 0.5$ fm/c.

For additional details on the numerical solution technique of the BNV equation we direct the reader to previous papers [1–11] and references therein.

4 Subthreshold π_0 production in Nb + Nb reaction

A technical problem in treating subthreshold pion production within the BNV model is that the numerical statistics from a straightforward use of the elementary cross-section would be very poor. Thus, we deal with this problem by calculating, at each test particle collisions of interest, the production probability and sum incoherently over these collisions in the whole nucleus-nucleus collisional event. In the perturbative approach [15], the recoil momentum for the final nucleons in the calculation of the time evolution of the heavy-ion system is then neglected. Within this picture, the Lorentz-invariant triple differential pion production cross-section, at a fixed impact parameter b is given by the sum of all possible nucleon-nucleon collisions of interest with the Pauli blocking for the final nucleon

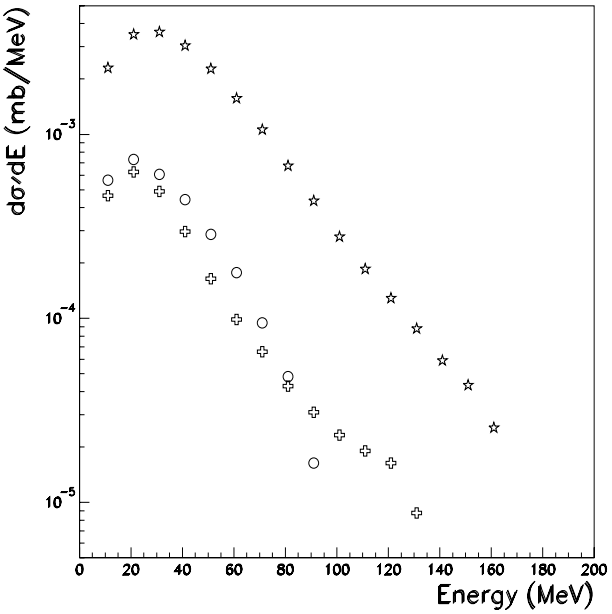

Fig. 5. Differential cross-sections for π_0 production in the ^{93}Nb + ^{93}Nb reaction at $E_{\rm lab} = 100$ A MeV. Comparison is shown between the results obtained using the local Skyrme potential (soft and hard EoS) and the microscopic momentum-dependent (MD) mean field. Stars refer to the calculations with the microscopic mean field, circles to soft Skyrme interaction and crosses to hard Skyrme interaction.

states taken into account

$$\frac{1}{p_\pi}\frac{\mathrm{d}^3\sigma_\pi}{\mathrm{d}E_\pi \mathrm{d}\Omega_\pi \mathrm{d}b} = 2\pi b \sum_{NN\mathrm{coll}(b)} \int \frac{\mathrm{d}\Omega_q}{4\pi}\frac{1}{p'_\pi}\frac{\mathrm{d}^2 P^{\mathrm{elem}}_{NN\pi}}{\mathrm{d}E'_\pi \mathrm{d}\Omega'_\pi} P_B P_{\mathrm{esc}}\,. \tag{13}$$

The primed and unprimed parameters denote quantities in the individual NN center-of-mass and laboratory frames, respectively. Ω_q is the solid angle of the relative momentum between the final nucleons which is not fixed by energy and momentum conservation and has to be averaged out. $P^{\mathrm{elem}}_{NN\pi}$ represents the π production probability in an elementary NN collision, P_B is the final-state Pauli-blocking factor determined from the occupation probabilities of the final nucleons in the phase space and P_{esc} represents the pion escape probability. The $P^{\mathrm{elem}}_{NN\pi}$ probability has been evaluated using for the nucleon-nucleon collisions the free N-N cross-section whose energy and angular dependence has been properly accounted for [15]. For the elementary $NN \to N'N'\pi$ probability, we used the parametrization of ref. [15]. While a consistent treatment of pion reabsorption in the subthreshold region has not yet been achieved, we introduce a phenomenological approach of ref. [16]. Whenever a pion is created, we follow its path inside the nuclear medium assuming it moves on a straight line determined by its momentum $\vec{p}_\pi$. Thus, the pion has to travel, inside the nuclear region, an effective distance dynamically depending on the surrounding medium and given by

$$\mathrm{d}(\vec{r}_\pi, \hat{p}_\pi, t) = \frac{1}{\rho_0}\int_0^{+\infty} \rho(\vec{r}_\pi + \hat{p}_\pi s, t)\mathrm{d}s\,, \tag{14}$$

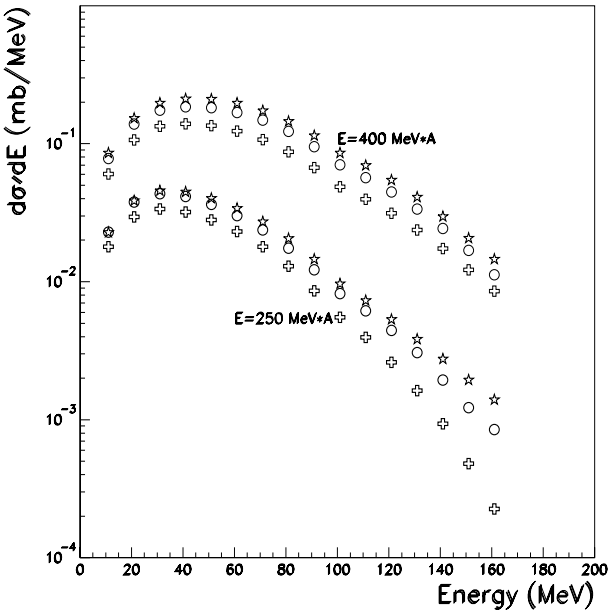

Fig. 6. Differential cross-sections for π_0 production in the ^{93}Nb +^{93} Nb reaction at $E_{\rm lab} = 250, 400$ A MeV. As in fig. 4, comparison is shown between the results obtained using the local Skyrme potential (soft and hard EoS) and the microscopic momentum-dependent mean field. The meaning of the symbols is the same as in fig. 4.

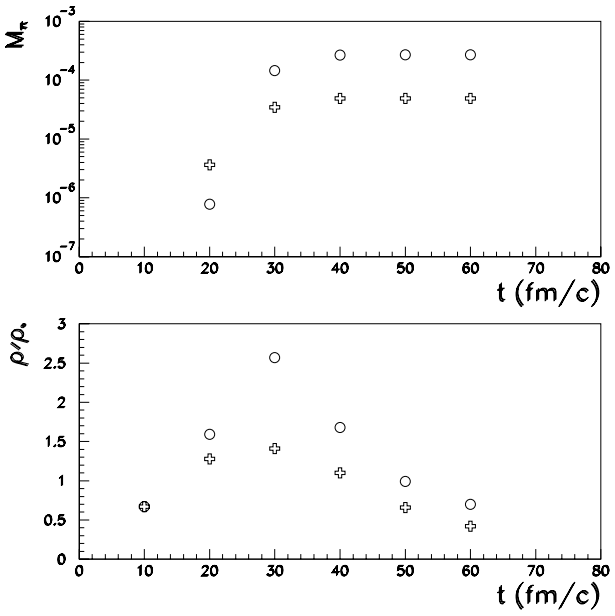

Fig. 7. Top: π_0 production multiplicity *vs.* collision time and bottom: ratio ρ/ρ_0 *vs.* collision time in the ^{93}Nb +^{93} Nb reaction at $E_{\rm lab} = 100$ A MeV. The circles refer to the case of the momentum-dependent microscopic mean field, while the crosses to the case of a soft local Skyrme potential.

where $(\vec{r}_\pi,\ t)$ are the pion production space-time coordinates, ρ is the nucleons density and ρ_0 its saturation value for the normal nuclear matter. The escape pion probability is then given by $P_{\rm esc} = \exp(-d/\lambda_0)$, where $\lambda_0 = (\sigma_{\rm abs}\rho_0)^{-1}$ represents the mean absorption lenght in normal nuclear matter. Both optical model [17] and transport [18] calculations predict a pion absorption mean free path which is dependent on the pion energy. For our calculation we have used a parametrization of the energy dependence of λ_0 given in ref. [18].

In the framework of the BBG approach the in-medium cross-section can be self-consistently calculated with the mean field by means of the G-matrix [19–22].

In figs. 5 and 6 the differential cross-sections for π_0 production are reported for three different energies. In fig. 5 the results for the case of $E_{\rm lab} = 100$ A MeV are reported. In fig. 6 the case of $E_{\rm lab} = 250, 400$ A MeV is considered. Comparison is shown between the results obtained using the local Skyrme potential and the microscopic momentum-dependent mean field. It is very clear the effect of the momentum dependence at low energy. At 100 MeV the cross-section is about 6–7 times larger when the MD potential is used. The difference is not so large when the bombarding energy increases, even if still appreciable. By integrating the differential cross-section of fig. 5 with the MD potential option we produce a total π_0 production cross-section equal to 0.2 mb, which is in quite good agreement with the expected extrapolated trend of experimental data [23]. Thus, the large enhancement (of a factor of 7, or so) produced by the MD potential goes in the right direction, even if a slightly larger value of the calculated total production cross-section should be in order to better agree with the extrapolated experimental trend at $E_{\rm lab} = 100$ A MeV.

The pion multiplicity *vs.* time, at $E_{\rm lab} = 100$ A MeV during the collision is shown in fig. 7, upper panel. The calculated density, actually ρ/ρ_0, *vs.* collision time is given in fig. 7, lower panel. The pion multiplicity reaches a saturating plateau at $t = 30$ fm/c, when the compression has a maximum. Again the calculations with MD mean field are compared with those using a soft Skyrme local potential. The same type of comments as above applies. The π_0 production shows an enhancement in the early stages of the collisions when the colliding nuclei explore a fast compression phase. The specific momentum and density dependences of the mean field are responsible for the observed enhancement of the pion multiplicity.

In conclusion, in this work we have reported kinetic calculations about π_0 production using a microscopic MD mean field. We have found that pion production is a very sensitive probe to the EoS entering the calculations, especially when the bombarding energy per nucleon is below the NN threshold. In particular, at $E_{\rm lab} = 100$ A MeV, the total pion cross-section for the momentum-dependent mean field is about a factor 7 larger than the corresponding value obtained with a local (soft and hard) Skyrme potential. This enhancement is in agreement with the observed trend of experimental data and also with the conclusions from kaon production calculations [19,24].

References

1. J. Aichelin, A. Rosenhauer, G. Peilert, H. Stoecker, W. Greiner, Phys. Rev. Lett. **58**, 1926 (1987).
2. C. Gale, G. Bertsch, S. Das Gupta, Phys. Rev. C **35**, 1666 (1987).
3. M. Baldo, I. Bombaci, L.S. Ferreira, G. Giansiracusa, U. Lombardo, Phys. Lett. B **209**, 135 (1988).
4. I. Bombaci, U. Lombardo, Phys. Rev. C **44**, 1892 (1991).
5. I. Bombaci, T.T.S. Kuo, U. Lombardo, Phys. Rep. **242**, 165 (1994).
6. J.P. Jeukenne, A. Lejeune, C. Mahaux, Phys. Rep. C **25**, 83 (1976).
7. M. Baldo, *BBG approach to the many body problem*, in *Nuclear Methods and Nuclear Equation of State*, edited by M. Baldo (World Scientific, Singapore, 1999) pp. 458-510.
8. J. Hüfner, C. Mahaux, Ann. Phys. (N.Y.) **73**, 525 (1972).
9. W. Zuo, I. Bombaci, U. Lombardo, Phys. Rev. C **60**, 024605 (1999).
10. R.B. Wiringa, R.A. Smith, T.L. Ainsworth, Phys. Rev. C **29**, 1207 (1984).
11. A. Insolia, U. Lombardo, N. Sandulescu, A. Bonasera, Phys. Lett. B **334**, 12 (1994)
12. M. Baldo *et al.*, Phys. Rev. C **41**, 1748 (1990)
13. Cheuk-Yin Wong, Phys. Rev. C **25**, 1460 (1982); C. Gregoire, B. Remaud, F. Sebille, L. Vinet, Y. Raffray, Nucl. Phys. A **465**, 317 (1987).
14. A. Bonasera, F. Gulminelli, J. Molitoris, Phys. Rep. **243**, 1 (1994).
15. A. Bonasera, G. Russo, H.H. Wolter, Phys. Lett. B**246**, 337 (1990).
16. A. Badalá, R. Barbera, A. Palmeri, G.S. Pappalardo, F. Riggi, A.C. Russo, G. Russo, R. Turrisi, C. Agodi, R. Alba, G. Bellia, R. Coniglione, A. Del Zoppo, P. Finoccchiaro, C. Maiolino, E. Migneco, P. Piattelli, P. Sapienza, A. Peghaire Phys. Rev. C **48**, 2350 (1993).
17. R.A. Mehrem, H.M.A. Radi, J.O. Rasmussen, Phys. Rev C **30**, 301 (1984); P. Hecking, Phys. Lett. B **103**, 401 (1981).
18. J. Huefner, M. Thies, Phys. Rev. C **20**, 273 (1979).
19. W. Cassing, U. Mosel, Prog. Part. Nucl. Phys. **25**, 253 (1990).
20. J. Cugnon, A. Lejeune, P. Grangé, Phys. Rev. C **35**, 861 (1987).
21. J. Jaenicke, J. Aichelin, N. Ohtsuka, R. Linden, A. Faessler, Nucl. Phys. A **536**, 201 (1992).
22. G.Q. Li, R. Machleidt, Phys. Rev. C **48**, 1702 (1993).
23. P. Braun-Munzinger, J. Stachel, Annu. Rev. Nucl. Part. Sci. **37**, 97 (1987)
24. U. Mosel, Annu. Rev. Nucl. Part. Sci. **41**, 29 (1991).